Applied Geochemistry xxx (2015) xxx–xxx

Contents lists available at ScienceDirect

Applied Geochemistry

journal homepage: www.elsevier.com/locate/apgeochem

Two sides to every range: Orographic influences on CO_2 consumption by silicate weathering

Brandon C. McAdams [a,b,*], Annette M. Trierweiler [a,b,1], Susan A. Welch [a,b], Carla Restrepo [c], Anne E. Carey [a,b]

[a] School of Earth Sciences, The Ohio State University, 275 Mendenhall Laboratory, 125 South Oval Mall, Columbus, OH 43210-1398, United States
[b] Byrd Polar and Climate Research Center, The Ohio State University, 1090 Carmack Road, Columbus, OH 43210-1002, United States
[c] Department of Biology, University of Puerto Rico-Rio Piedras, P.O. Box 23360, San Juan, PR 00931-3360, United States

ARTICLE INFO

Article history:
Available online xxxx

ABSTRACT

The effect of an orographic rain shadow on CO_2 consumption by silicate weathering ($ØCO_{2,Si}$) was examined in the Sierra de Las Minas, a mountain range in eastern Guatemala. This range is tall enough to intercept prevailing winds, leading to greater rainfall on the windward or north compared to the leeward or south side of the range. Water was collected from and discharge was measured for streams draining both the north and south sides of the Sierra de Las Minas. Water samples were analyzed for major ions and silica and this chemistry was used to interpret weathering inputs and calculate $ØCO_{2,Si}$. The median $ØCO_{2,Si}$ in north side streams (260×10^3 mol CO_2 km^{-2} yr^{-1}) was roughly 3-fold greater than the median $ØCO_{2,Si}$ in south side streams (78×10^3 mol CO_2 km^{-2} yr^{-1}). This difference is similar to the 3-fold greater discharge measured for north side streams compared to south side streams of the same area. A positive linear relationship was observed between volumetric water yield (L s^{-1} km^{-2}) and $ØCO_{2,Si}$, supporting transport (i.e. precipitation) as the main factor controlling the differences observed between north and south side $ØCO_{2,Si}$. Lithology and basin morphology differences had a negligible influence on $ØCO_{2,Si}$ patterns across the aspects of the range. These orographically induced differences in $ØCO_{2,Si}$ may increase with changing precipitation regimes in a warming climate.

1. Introduction

Through a combination of circumstances—range profile and aspect, wind direction and velocity, air temperatures, atmospheric currents—mountain ranges around the world experience an orographic rain shadow that creates a dry leeward side and a wet windward side of the range (Barros and Lettenmaier, 1994; Galewsky, 2009; Houze, 2012). The impact of rain shadows on erosion rates, uplift, and range and stream morphology has been observed and modeled (Willett, 1999; Roe et al., 2002; Menking et al., 2013). However, significant impacts of rain shadows on CO_2 consumption from silicate chemical weathering have been little observed (Gaillardet et al., 2011).

Orogenic events play major roles in global CO_2 concentrations over geologic time by catalyzing chemical weathering and transport processes within mountain watersheds (Berner et al., 1983; Stallard and Edmond, 1983; Francois and Walker, 1992; Milliman and Syvitski, 1992; Raymo and Ruddiman, 1992; Berner, 1994; Raymo, 1994; Averbuch et al., 2005; West et al., 2005). Contemporary studies of mountain watersheds have observed disproportionate contributions to global chemical weathering and organic carbon transport in small mountainous rivers relative to their size (Milliman and Syvitski, 1992; Lyons et al., 2002; Carey et al., 2005a,b, 2006; Goldsmith et al., 2008a,b). High chemical weathering rates in mountain watersheds have been attributed to the exhumation of fresh bedrock by the high physical weathering rates observed in mountain catchments (Riebe et al., 2001, 2004; Anderson et al., 2002; Millot et al., 2002; Jacobson and Blum, 2003; Carey et al., 2005b; Lyons et al., 2005; Goldsmith et al., 2008a).

New mineral surfaces are created through physical weathering processes and resetting events that break apart and redistribute or refresh rock surfaces (Vitousek et al., 1997; Filipelli and Souch, 1999). The extent of bedrock sediment redistribution and exposure to the hydrosphere dictates the influence any physical

* Corresponding author at: School of Earth Sciences, The Ohio State University, 275 Mendenhall Laboratory, 125 South Oval Mall, Columbus, OH 43210-1398, United States. Tel.: +1 614 354 0524.

E-mail addresses: mcadams.25@osu.edu (B.C. McAdams), atrierwe@princeton.edu (A.M. Trierweiler), welch.318@osu.edu (S.A. Welch), crestre@hpcf.upr.edu (C. Restrepo), carey.145@osu.edu (A.E. Carey).

[1] Current address: Department of Ecology and Evolutionary Biology, Princeton University, 106A Guyot Hall, Princeton, NJ 08544, United States.

http://dx.doi.org/10.1016/j.apgeochem.2015.04.010
0883-2927/

weathering—secondary generation of reactive mineral surfaces—will have on chemical weathering in the watershed (West et al., 2005). Although two watersheds may experience similar amounts of physical weathering, they may not receive the same amount of rainfall. If no other factors are considered, then the amount of water is typically the limiting factor on the water–rock interactions that occur in a watershed (Filipelli, 1997; Stewart et al., 2001). However, this example ignores how the watersheds may differ in their geomorphology and how they function as basins to store (or transport) sediments and move water through (or store water within) these sediments (McGuire et al., 2005; Soulsby et al., 2006; Sayama and McDonnell, 2009; Maher, 2010, 2011; West, 2012). It is also possible that the geomorphology of a wet mountain catchment would reach a different stable state in terms of shape and function than that of a dry mountain catchment (Willett, 1999; Roe et al., 2002; Menking et al., 2013).

Lithology also influences the effect that chemical weathering within a watershed will have on the geologic carbon cycle (Bluth and Kump, 1994). Silicate chemical weathering and the subsequent precipitation of carbonate minerals from weathering's dissolution products is the only geologically long term mechanism by which carbon dioxide is removed from the atmosphere (Raymo and Ruddiman, 1992; Berner, 1994). Whereas watersheds draining carbonate lithologies lacking silicate minerals will not have an impact on the inorganic carbon cycle over geologic time (Berner et al., 1983). Therefore, it is necessary to account for carbonate weathering contributions to stream chemistry in order to calculate atmospheric CO_2 consumption yields of watersheds, or those yields resulting from silicate weathering, designated as $ØCO_{2,Si}$ adapted from Edmond and Huh (1997). However, silicate weathering rates can decrease over time as the surface of rocks are weathered and soils develop, diminishing the amount of fresh primary mineral surfaces interacting with the hydrosphere (Vitousek et al., 1997; Carey et al., 2005b). In some cases of extremely weathered substrates, silicate weathering may occur without affecting the inorganic carbon cycle vis a vis leaching of Si into solution with no contribution of cations and alkalinity to remove CO_2 from the atmosphere (Edmond et al., 1995; Edmond and Huh, 1997). In addition, weathering of volcanic lithologies, as in Gaillardet et al. (2011) may be very different than weathering of metamorphic lithologies, as reported herein.

Given the known influences of basin morphology and lithology on chemical weathering, these two factors were examined to elucidate the effects of precipitation on the following hypothesis: silicate weathering CO_2 consumption yields ($ØCO_{2,Si}$) are greater in rivers draining the wet, windward, north side of the Sierra de Las Minas than in rivers draining the dry, leeward, south side of the range.

2. Materials and methods

2.1. Study area

The Sierra de Las Minas, the subject of this study, are located in eastern Guatemala and are bordered by the Polochíc river valley to the north and the Motagua river valley to the south (Fig. 1a and b). The Sierra de Las Minas rise ~3000 m above sea level (Bucknam et al., 2001), an elevation high enough to intercept the prevailing tradewinds from the northeast and create a rain shadow on the south or leeside of the range (Campbell, 1982; Holder, 2006). This rain shadow creates a substantial difference in hydrologic budgets between the north and south sides of the Sierra de Las Minas. The mean annual areal distribution of rainfall on the north side of the range centers around 2400–2600 mm yr^{-1}, whereas mean annual precipitation shows two peaks on the south side, with roughly half centered around 1800–2600 mm yr^{-1} and a quarter centered around 800 mm yr^{-1} (Fig. 1c). Mean monthly discharges of rivers draining the north and south side of the range show a pronounced dry season from February through May (Fig. SI 1). The areal distribution of slope (degrees km^{-2}) is similar between the north and south sides of the range, showing a large peak at 0–5°, representing the valleys of the Motagua (south) and Polochíc (north) rivers (Fig. 1c). Slopes are also distributed around a second peak of 25–30° on the south side and 30–35° on the north side, a potential relative difference of 5–10° of slope (Fig. 1c). Mean annual temperature varies little from the north to the south side of the range (Fig. 1c).

The lithology of the north side of the Sierra de Las Minas is made up of the San Agustín formation (Paleozoic age, uplifted quartz-monzonite gneiss with various schists), the Santa Rosa group (a succession of fossiliferous shales Carboniferous to Permian in age representing a paleo-marine shelf), the Chóchal complex (Permian dolomite and limestone with some shale and minor conglomerate), and an unnamed Triassic granite formation (Bonis, 1967; Bonis et al., 1970; Weyl, 1980; Bundschuh and Alvarado, 2007; Fig. 1d). The San Agustín formation composes the core of the range and also crops out on the south side along with the Jones formation (a metasedimentary complex of phyllites and pelitic schists), the San Lorenzo formation (a massive fine grained marble), and other minor units (Bonis et al., 1970; Newcomb, 1975; Bundschuh and Alvarado, 2007; Fig. 1d and e).

2.2. Sampling and field measurements

Water samples were collected from 16 streams sites on the north side and 26 stream sites on the south side of the Sierra de Las Minas (Fig. 1d and e; Table 1). North side samples were collected from January to March 2012, and south side samples were collected during June and July 2009. A bulk rainwater sample was also collected on the north side of the range over a 9 week period from the end of January through the middle of March, 2012 at Finca la Constancia (15.300227N, 89.724101W, NAD83).

All water samples were kept in the dark after collection. Water samples collected from the north side of the range were either filtered or refrigerated within 24 h of collection. Most samples collected on the south side were filtered within 24 h of collection and all were filtered within 17 days of collection. Stream samples were filtered through 0.45 μm pore size Whatman Nucleopore™ filters directly into Nalgene™ low density polyethylene bottles using a polycarbonate filter tower and fritted polycarbonate funnel with a vacuum bell-jar after Lyons et al. (2005). Samples for cation analysis were acidified to a pH of 2–4 either immediately after filtering or just prior to analysis using either 1 N HCl or concentrated trace metal grade HNO_3.

Temperature and pH measurements were made at the sampling location using an Orion Star field meter, by inserting the probes either directly into the stream after sampling or into a 1 L plastic beaker filled with stream water if the flow was too turbulent for the meter to stabilize in the stream. Manual stream discharge measurements were made on both sides of the range. Stream flow measurements on the north side were recorded as the modal flow over a continuous minute of measurement by an OTT Acoustic Doppler Current meter. The velocity of streams on the south side was measured using a mechanical flow meter from General Oceanics Environmental Division. On both sides of the range, the USGS short term gauging method was followed (Rantz, 1982). Some streams were deemed unsafe to gauge manually and discharge was calculated using Eq. (2) or (3) derived from linear relationships between watershed area and discharge. Though discharge of five streams on the north side and four streams on the south side was measured

Please cite this article in press as: McAdams, B.C., et al. Two sides to every range: Orographic influences on CO_2 consumption by silicate weathering. Appl. Geochem. (2015), http://dx.doi.org/10.1016/j.apgeochem.2015.04.010

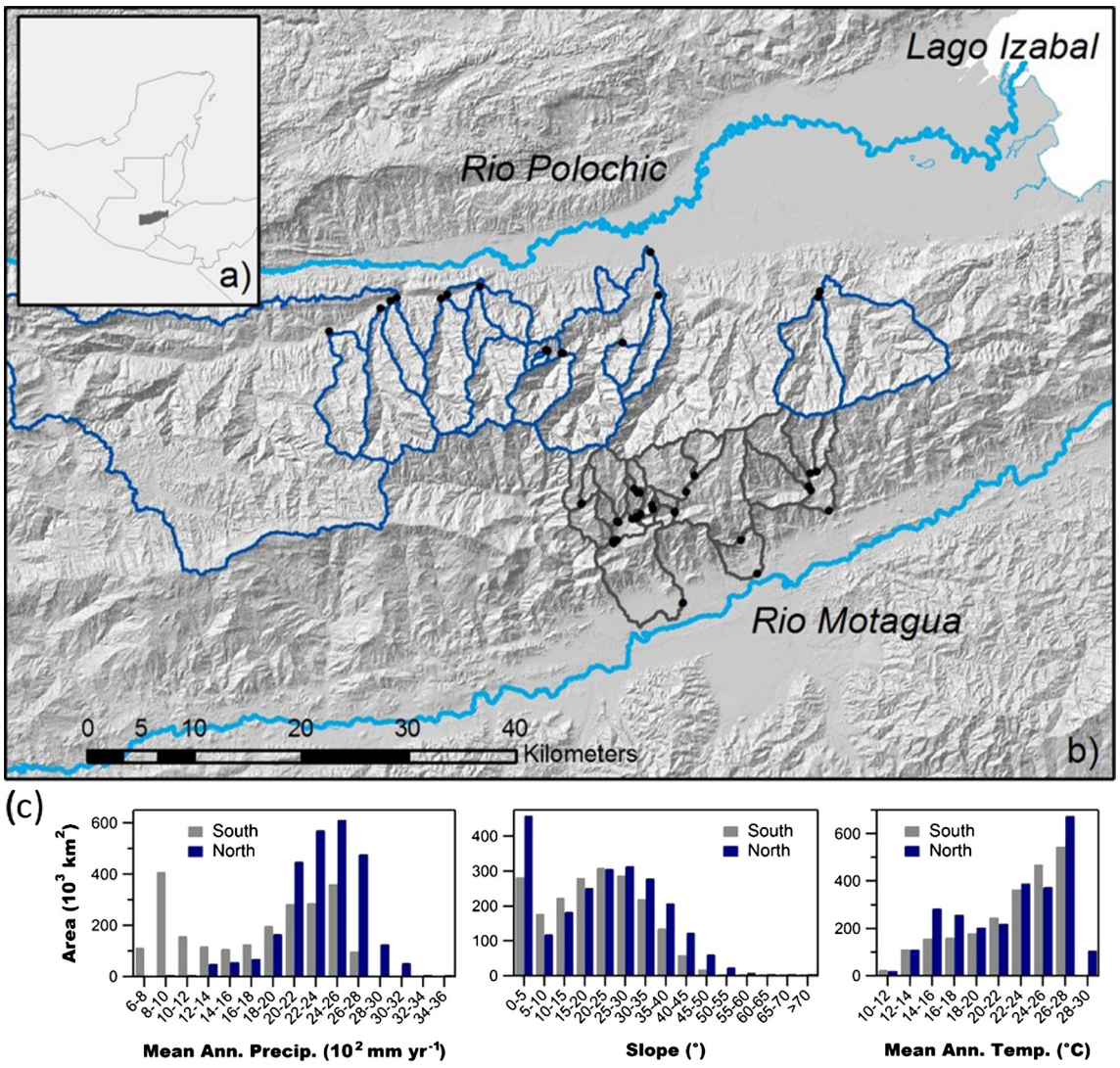

Fig. 1. (a) Location of Guatemala and Sierra de Las Minas (shaded portion) in Central America. (b) Basins sampled, blue outlines are north, Polochic side watersheds; black outlines are south, Motagua side watersheds. (c) Histograms of mean annual precipitation, slope, and mean annual temperature with area and categorized by aspect. (d) and (e) lithology of study area wherein (e) represents the rectangular outline in (d). Geologic units in (d) and (e) are as follows: Qal – Quaternary alluvium; KTsb – Cretaceous-Tertiary Subinal formation; Trgr – Triassic granite; Pc – Permian Chochál formation; Psr – Carboniferous-Permian Santa Rosa group; Pm/Psa – Paleozoic San Augustín gneiss; Tc – Chanchan formation; Tg – Tertiary Gustatoya formation; Pslm – Paleozoic San Lorenzo marble; Pj – Paleozoic Jones schist formation; Psa – Paleozoic San Augustín migmatite; S – Unknown age serpentenite. Numbers correspond to dots that show sampling locations as found in Table 1.

more than once, too few measurements were made to determine baseflow.

2.3. Analytical methods

Major ion concentrations of water samples were determined using a Dionex DX-120 Ion Chromatograph following the methods of Welch et al. (2010). Dissolved silica concentrations were measured on a Skalar SAN++ nutrient analyzer using the method supplied by the manufacturer. At least five analyses of 3–4 different standard concentrations were run as unknowns with each analytical run and showed accuracies of ±5% for major ion and silica analysis. Precision was determined by repeating both standards and samples at least five times over the course of a run and with precision of ±2%.

Alkalinities of north side streams were analyzed in the field using a Hach digital titration field kit with a bromcresol green/phenol phthalein indicator and a 0.01 N HCl solution in 20 mL of stream water. Alkalinities of south side streams were determined at a central location using the Gran titration method on the same day samples were collected. Charge balance errors averaged less than ±10%, including NO_3^- and PO_4 (Trierweiler, 2010; McAdams, 2012).

2.4. Geochemical input calculations from a mixing model

Because the Sierra de Las Minas are lithologically heterogeneous, a mixing model was employed to separate stream chemistry resulting from silicate weathering from that resulting from other sources (e.g. carbonate weathering, precipitation). Geochemical inputs to stream chemistry were calculated after a mixing equation defined by Gaillardet et al. (1999) to determine relative contributions of rainwater and weathering of silicate, carbonate, and evaporite minerals to stream chemistry. This approach has been modified by others to separate hydrothermal inputs from silicate weathering inputs (Goldsmith et al., 2010) and was modified here to reflect the lithology of the study area (Fig. 1d and e). All geochemical inputs to stream chemistry were assumed to result from

Please cite this article in press as: McAdams, B.C., et al. Two sides to every range: Orographic influences on CO_2 consumption by silicate weathering. Appl. Geochem. (2015), http://dx.doi.org/10.1016/j.apgeochem.2015.04.010

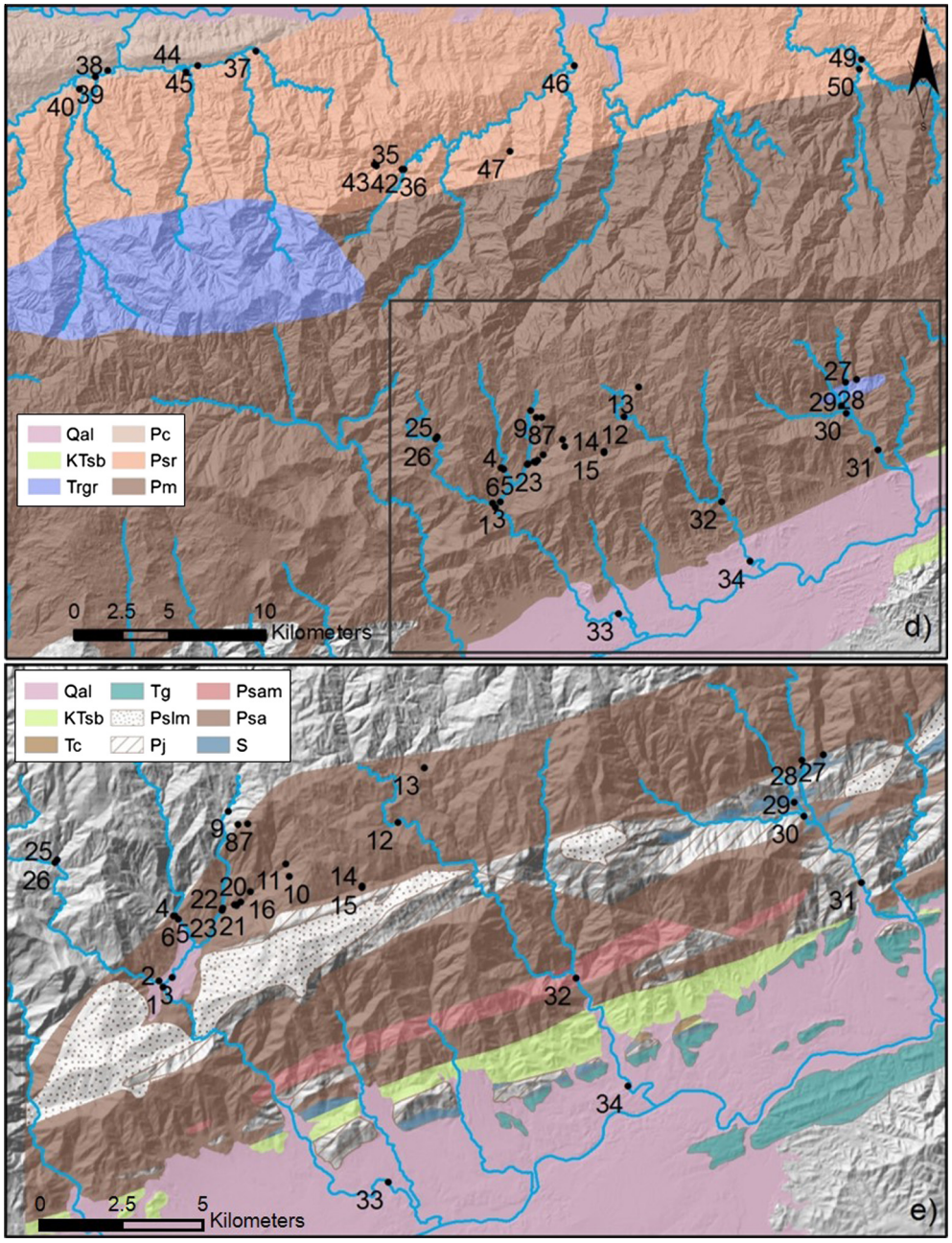

Fig. 1 (*continued*)

silicate weathering, carbonate weathering, or rainwater. The following mixing equation (after Gaillardet et al., 1999) was used to determine silicate weathering, carbonate weathering, and rainwater inputs to stream chemistry (for X = Ca, Mg, K, HCO_3, Cl, and SO_4):

$$(X/Na)_{river} = \alpha_{rain}(Na) * (X/Na)_{rain} + \alpha_{carbonate\ weathering}(Na) * (X/Na)_{carbonate\ weathering} + \alpha_{silicate\ weathering}(Na) * (X/Na)_{silicate\ weathering} \quad (1)$$

where α_i(Na) is the Na proportion derived from *i* = *rain*, *carbonate weathering*, or *silicate weathering* with $\alpha_{rain} + \alpha_{carbonate\ weathering} + \alpha_{silicate\ weathering} = 1$. These values are presented herein as α_{rain}, α_{carb}, and α_{Si}, respectively, and also as percentages so that their sum is 100. From Eq. (1), seven equations and 28 parameters were obtained for which all α_i(Na) values were the unknowns. Since the number of equations is greater than the number of unknowns, the system was over-constrained and a least squares inversion was used to calculate a solution in MATLAB R2011a. The resultant α_i values were then normalized to 1 and used to calculate the relative input of each component (*i*) into stream water where the percent input of (*i*) is equal to α_i multiplied by 100.

Ratios of $(X/Na)_i$ for *i* = *carbonate weathering* and *i* = *silicate weathering* were chosen from a range of values presented by Gaillardet et al. (1999) (Table SI 1) and were selected to calculate silicate weathering input conservatively by using the low values of for carbonate weathering end member. In this way, the percentage of input calculated from carbonate weathering is more sensitive to increases in stream water values of Ca/Na, Mg/Na, and HCO_3/Na greater than those expected for silicate weathering or rain. For *i* = *rain*, $(X/Na)_{rain}$ were the ratios in the bulk rainwater sample (Table SI 1).

Please cite this article in press as: McAdams, B.C., et al. Two sides to every range: Orographic influences on CO_2 consumption by silicate weathering. Appl. Geochem. (2015), http://dx.doi.org/10.1016/j.apgeochem.2015.04.010

Table 1
Physical characteristics of watersheds.

Sample site	Latitude[c]	Longitude[c]	Elevation (m)	Stream order	A (km^2)	Sample number[b]
South side streams						
Trib. 1 to El Ingles	0211993	1670658	1648	1st	0.16	10
Trib. 2 to El Ingles	0211890	1671019	1613	1st	0.21	11
Trib. 3 to El Ingles	0210454	1669858	1219	2nd	1.2	18
Q. Bejucal	0214075	1670353	1564	2nd	2.4	14
Q. Picacho	0214075	1670153	1555	2nd	2.8	15
El Portón 1[a]	0210259	1672577	1941	2nd	3.2	9
R. El Ingles 1	0210464	1669885	1237	3rd	3.7	19
Q. Blanca	0205295	1671259	1719	3rd	4.0	25
R. El Manguito	0208643	1669584	1141	3rd	4.2	4
R. El Ingles 2	0210408	1669877	1231	3rd	4.9	20
R. El Ingles 3	0210067	1669774	1149	3rd	5.3	21
R. La Lima	0227391	1673927	742	3rd	7.2	27
El Portón 2	0210050	1669769	1163	3rd	7.6	22
R. El Chorro 1	0205265	1671176	1740	3rd	8.9	26
R. Veguita	0215845	1673741	1811	3rd	10	13
R. Blanco	0226796	1673717	672	3rd	12	28
El Portón 3	0210041	1669718	1141	4th	13	23
R. Repollal 1	0208673	1669580	1084	4th	15	5
R. Colorado	0226547	1672572	567	4th	17	29
R. Repollal 2	0208790	1669492	1058	4th	19	6
R. Agua Fría	0215141	1672142	1654	4th	20	12
R. El Chorro 2	0208196	1667722	909	4th	23	2
R. Cañas	0226930	1672272	584	4th	24	30
R. Pasabién 1	0208578	1667822	910	5th	36	3
R. Pasabién 2	0208305	1667522	892	5th	60	1
R. Jones	0228418	1670208	346	5th	72	31
R. Hondo 1	0220185	1667600	313	5th	80	32
R. Hondo 2	0221627	1664468	180	5th	93	34
R. Pasabién 3	0214691	1661820	212	5th	105	33
North side streams						
Trib. 2 to Chajonja	0202257	1685644	783	1st	0.35	43
Trib. 1 to Chajonja	0202349	1685564	810	1st	1.2	42
Q. Chajonja	0203705	1685359	611	3rd	7.1	36
Q. Cancor	0209502	1685998	246	3rd	7.2	47
Q. Carabajal	0196144	1691700	331	3rd	15	37
R. Chiquito	0212848	1690636	125	3rd	18	46
R. Sibija	0187709	1690469	162	4th	18	39
R. Raxon	0203793	1685324	582	4th	24	35
R. Pancajoc	0181960	1687755	205	4th	38	41
R. Toila	0192453	1690654	231	4th	42	44
R. Tze	0227778	1690204	206	4th	46	50
R. Mululha	0186861	1689833	184	4th	52	40
R. Samilja	0193094	1690972	203	4th	67	45
R. Zarco	0227914	1690729	185	5th	83	49
R. Pueblo Viejo	0212104	1694610	28	5th	140	48
R. Matanzas	0188359	1690769	143	6th	590	38

[a] Numbers following sample sites increase from upstream (e.g. 1) to downstream (e.g. 2, 3) locations for the same stream.
[b] Sample numbers correspond with labels in Fig. 1.
[c] Based on NAD83 datum, section 16P.

2.5. Calculations of CO_2 consumption from silicate weathering ($ØCO_{2,Si}$)

Silicate weathering CO_2 consumption ($ØCO_{2,Si}$) was calculated by two approaches from Edmond and Huh (1997), presented proportionally as (1) $ØCO_2 = ØALK$ and (2) $ØCO_2 = 2.ØSi$ (algebraically as $ØCO_2 = ØSi/2$). The prefix Ø to a variable (CO_2, ALK, or Si) signifies yields of that variable and so implies multiplication by a discharge (Q) and division by a watershed area (A) to achieve molar or equivalent units of the variable per area per time (Edmond and Huh, 1997). Yields are generally presented as mol km^{-2} yr^{-1} (e.g. Edmond and Huh, 1997; Gaillardet et al., 1999, 2011; Lyons et al., 2005; Carey et al., 2006; Goldsmith et al., 2008b, 2010). Others have shown annual yields calculated for a watershed made from a single sample or a handful of repeat samples can be adequately representative (e.g. Lyons et al., 2005; Goldsmith et al., 2008b).

To calculate silicate weathering derived HCO_3^-, concentrations were multiplied by $a_{silicate\ weathering}$ (α_{Si}) as calculated by the mixing model in Section 2.4. The model corrected concentrations of HCO_3^- were assumed to represent alkalinity derived from silicate weathering (ALK_{Si} in μmol L^{-1}), though some exceptions were found (Section 3.3). All Si was assumed to be from silicate weathering and so did not require model correction. Conversion from concentration to yields provided $ØALK_{Si}$ and ØSi. These yields are then used to calculate $ØCO_2$ from silicate weathering ($ØCO_{2,Si}$). Comparison of these two approaches provided information about relative differences between carbonate and silicate weathering that were not elucidated by the mixing model presented in Section 2.4 (Section 3.3).

3. Results

3.1. Watershed area and stream discharge

Watershed areas upstream of sampling locations range from 0.35 km^2 to 700 km^2 for north side catchments and from 0.05 km^2 to 106 km^2 for south side catchments (Table 1). Any north

Please cite this article in press as: McAdams, B.C., et al. Two sides to every range: Orographic influences on CO_2 consumption by silicate weathering. Appl. Geochem. (2015), http://dx.doi.org/10.1016/j.apgeochem.2015.04.010

side stream where discharge was not measured had a watershed area greater than 24 km^2. Measured discharges ranged from 18 L s^{-1} to 1800 L s^{-1} ($n = 18$) for north side streams and from 0.1 L s^{-1} to 1800 L s^{-1} ($n = 21$) for south side streams. There was a positive linear correlation between measured stream discharge (Q, in L s^{-1}) and watershed area (A, in km^2) for both north and south side streams. These relationships are described by the following Eqs. (2) and (3) for north and south side streams (labeled Q_N and Q_S, respectively):

$$Q_N = 44A + 42 \quad (n = 18,\ r^2 = 0.66,\ p < 0.01) \tag{2}$$

$$Q_S = 16A - 6 \quad (n = 21,\ r^2 = 0.95,\ p \ll 0.01) \tag{3}$$

The slopes of the regression lines suggest that a north side stream will have roughly 3-fold more water moving through it than a south side stream of the same area. For R. Matanzas, the largest north side watershed, discharge extrapolated from Eq. (3) (26,000 L s^{-1}) is similar to the median of mean daily discharges recorded by Instituto Nacíonal de Sismología, Vulcanología, Meteorología e Hidrología of Guatemala (personal communication) over a 7 year period from 2003 to 2010 (27,000 L s^{-1}; Fig. SI 2).

3.2. Stream geochemistry

River temperatures ranged from 15.9 °C to 25.4 °C in north side streams and from 14.8 °C to 28.9 °C in south side streams (Table SI 2). The pH of stream waters ranged from 6.19 to 8.17 on the north side of the range and from 6.45 to 8.50 on the south side (Table 2). Major cation concentrations in north and south side streams were generally dominated by Na^+ followed by Ca^{2+}, although 10 streams had higher Ca^{2+} than Na^+ concentrations (Table SI 2). Median concentrations of Ca^{2+} and Mg^{2+} were similar on the north and south side of the range (56.9 and 28.8 μM compared to 59.6 and 33.3 μM, respectively; Table 2). However, the highest Ca^{2+} and Mg^{2+} concentrations were observed in south side streams (Tables 2 and SI 2). South side streams also had the highest Na^+ and K^+ concentrations (Tables 2 and SI 2), and the median Na^+ and K^+ concentrations in south side streams are more than twice the median concentrations of Na^+ and K^+ in north side streams (178 and 27.5 μM compared to 88.8 and 12.1 μM, respectively; Table 2). Bicarbonate was the most abundant anion in all streams, ranging from 68.1 to 712 μM on the north side of the range and from 88.0 to 2365 μM on the south side of the range (Table 2). South side streams had a greater median HCO_3^- concentration than north side streams (323 μM compared to 231 μM, respectively; Table 2). Silica concentrations ranged from 192 to 873 μM in north side streams and from 26 to 540 μM in south side streams (Table 2). North side streams had a greater median Si concentration than south side streams (454 μM compared to 326 μM, respectively; Table 2). No correlation was observed between temperature and silica concentrations for either side of the range ($r^2 = 0.04$ and 0.19, north and south, respectively), implying no significant temperature effect on silicate weathering in these streams.

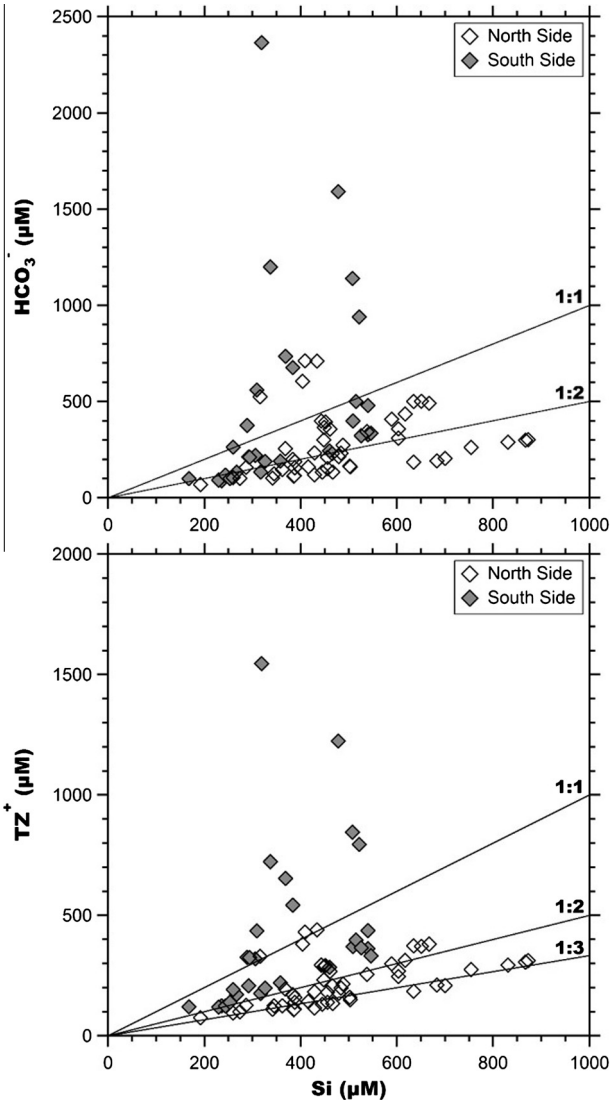

Fig. 2. HCO_3^- and TZ^+ vs. Si for north and south side streams. Lines drawn represent HCO_3^-:Si and TZ^+:Si ratios as indicated by the labels above each line.

Stream pH values were generally more basic in streams where Ca^{2+} was the dominant cation, and all streams where pH > 8 were dominated by Ca^{2+} (Table SI 2). Most streams with Ca^{2+} as the dominant cation drained areas underlain in part by mapped carbonate lithologies—either the Chóchal complex on the north side or the San Lorenzo marble on the south side—except for R. El Manguito,

Table 2
Median and ranges of discharge, pH, and major ion chemistry for north and south side streams.

			Concentrations (μM)								
	Q (L s^{-1})	pH	Ca^{2+}	Mg^{2+}	Na^+	K^+	HCO_3^-	Cl^-	SO_4^{2-}	Si	TZ^+
North side streams, n = 50											
Median	1700	7.41	56.9	28.8	88.8	12.1	231	15.1	10.7	454	203
Min	18	6.19	16.3	4.2	46.9	3.7	68.1	8.2	3.6	192	74.9
Max	26,000	8.17	232	121	199	21.0	712	24.9	24.8	873	440
South side streams, n = 29											
Median	203	7.61	59.6	33.3	178	27.5	323	28.7	11.5	326	326
Min	2.6	6.45	15.9	5.4	65.2	14.5	88.0	13.0	4.6	168	119
Max	1802	8.50	1090	246	341	64.0	2365	65.5	41.0	546	1546

Please cite this article in press as: McAdams, B.C., et al. Two sides to every range: Orographic influences on CO_2 consumption by silicate weathering. Appl. Geochem. (2015), http://dx.doi.org/10.1016/j.apgeochem.2015.04.010

Q. Chajonja, and Q Cancor (Fig. 1d and e; Table SI 2). R. El Manguito was also the only stream saturated with respect to calcite and dolomite (SI_{cal} = 0.14, SI_{dol} = 0.09; Table SI 2). Most other streams near calcite and dolomite saturation ($0 > SI_{cal,dol} > -1$) were dominated by Ca^{2+}, with the exception of R. Colorado (Table SI 2). Q. Chajonja and Q. Cancor were the only streams where Ca^{2+} was the dominant cation, but $SI_{cal,dol} < -1$ (Table SI 2). Those streams with calcite and dolomite saturation indices <−1, high pH and Ca^{2+}, and carbonate bedrock within their watersheds reflected influences by carbonate weathering.

Ratios of TZ^+ and of HCO_3^- to Si were examined to explore potential influences of carbonate weathering on stream chemistry (Fig. 2). Garrels (1967) found that rivers draining a variety of igneous and metamorphic rocks had HCO_3^-:Si ratios between 0.1 and 1.0 with most values falling between 0.3 and 0.5. Edmond and Huh (1997) stated that these HCO_3^-:Si ratios are essentially TZ^+:Si and reflect an estimated ratio for silicate weathering from a global data set (Berner et al., 1983). Thus streams with TZ^+:Si and HCO_3^-:Si ratios above 0.5 may have been influenced by carbonate weathering and streams with TZ^+:Si and HCO_3^-:Si ratios above 1 were almost certainly influenced by carbonate weathering (Fig. 2; Table SI 2). Those streams that plot farther above the 1:1 lines are also those streams with $SI_{cal,dol} > -1$, high pH and Ca^{2+}, and have carbonate bedrock mapped in their watersheds (Figs. 1d and e & 2; Table SI 2). For carbonate influenced streams, $ØCO_{2,Si}$ calculated from alkalinity may overestimate actual CO_2 consumption yields from silicate weathering, depending of the efficacy of the mixing model (Section 2.4) to account for carbonate weathering. To decrease dependence on the mixing model, 2.ØSi was deemed the best conservative calculation of $ØCO_{2,Si}$ for streams with carbonate influences (Tables SI 2 and SI 3).

Ratios of TZ^+:Si also provide information about the weathering regimes of watersheds. Specifically, Edmond et al. (1995) found low TZ^+:Si ratios (≤1:3) to represent the weathering of secondary clay minerals (e.g. montmorillonite, kaolinite) that contribute Si to stream chemistry without contributing cations or alkalinity. The recognition of such an environment is important for calculating $ØCO_{2,Si}$ from streams because, in these cases, calculations of $ØCO_{2,Si}$ by 2.ØSi would overestimate actual CO_2 consumption yields. Therefore, for those streams that fall near or below the 1:3 TZ^+:Si line (Fig. 2), $ØALK_{Si}$ was considered the best conservative calculation of $ØCO_{2,Si}$ (Tables SI 2 and SI 3).

3.3. $\alpha_{Si,rain,carb}$ and $ØCO_{2,Si}$

Median and maximum α_{Si} values—presented as percentages—were similar on the north and south sides of the range (91.1 and 98.1 compared to 88.8 and 98.5, respectively; Table 3). However, the minimum α_{Si} value on the south side of the range, 31.8, was much lower than the minimum α_{Si} on the north side of the range, 79.3 (Table 3). Conversely, the maximum α_{rain} and α_{carb} values on the south side of the range were much greater than those for the north side of the range (42.3 and 25.9 compared to 18.3 and 16.1, respectively). The lowest south side α_{Si} value and highest south side α_{rain} and α_{carb} were calculated for Q. Picacho (Table SI 3), a sample site proximally downstream from a marble quarry. Contributions from the marble quarry may have influenced input calculations for Q. Picacho. However, any influences did not affect $ØCO_{2,Si}$ calculations for Q. Picacho as 2.ØSi was used to calculate $ØCO_{2,Si}$. Streams with the highest α_{carb} values on either side of the range were also those streams with chemistry representative of carbonate weathering influences (Section 3.2; Table SI 3) and where $ØCO_{2,Si}$ was calculated as 2.ØSi. For these streams with chemistry characteristic of carbonate weathering influences where $ØCO_{2,Si}$ was calculated as 2.ØSi, $ØALK_{Si}$ was between 115% and 508% greater than 2.ØSi (Table SI 3). These large differences between $ØALK_{Si}$ and 2.ØSi suggest that the input model may have under calculated α_{carb} (and thus over calculated α_{Si}) for these streams by 30–70% (or the difference between 2.ØSi:$ØALK_{Si}$ and α_{carb}). For streams where carbonate influences were not so pronounced, but $ØALK_{Si}$ was greater than 2.ØSi, 2.ØSi provided the best conservative approach to calculating $ØCO_{2,Si}$. In this way, influences from unmapped carbonate units or disproportionate contributions of minor carbonate phases to stream chemistry (as observed by Jacobson et al. (2003) in New Zealand streams) were thought to be removed from $ØCO_{2,Si}$.

Although more south side than north side streams had pronounced carbonate weathering influences to stream chemistry (Section 3.2), the median α_{carb} of north side streams was greater than the median α_{carb} of south side streams. Nearly all north side streams drain portions of the Santa Rosa group, a fossiliferous shale unit that probably contributed carbonate weathering solutes to north side streams, whereas many south side watersheds have no known carbonate bearing bedrock (Fig. 1d and e). With the exception of R. Matanzas, R. Zarco, Q. Chajonja, and Q. Carabajal, 2.ØSi in all north side streams was greater than $ØALK_{Si}$, and for eight south side streams, 2.ØSi was greater than $ØALK_{Si}$ (Table SI 3). On the north side, only the R. Matanzas watershed comprised known carbonate bearing bedrock, the Chóchal formation (Section 2.1; Fig. 1d). Many north side streams show evidence of secondary mineral weathering (Section 3.2) that may reflect a highly weathered substrate and/or influences from the Santa Rosa shale. In all cases where 2.ØSi is greater than $ØALK_{Si}$, 2.ØSi may reflect weathering of secondary clay minerals that would not contribute alkalinity to stream chemistry and thus have no real effect on $ØCO_{2,Si}$ (Edmond et al., 1995). Thus, $ØALK_{Si}$ was considered the best conservative estimate of $ØCO_{2,Si}$ for these streams.

The median of the best conservative $ØCO_{2,Si}$ in north side streams was roughly 3-fold greater than the median for south side streams (260 compared to 78×10^3 mol CO_2 km^{-2} yr^{-1}, respectively; Table 3). This difference is similar to the difference in slopes of regression Eqs. (2) and (3) from the linear relationships between watershed area and discharge for both sides of the range (Section 3.1). The median $ØCO_{2,Si}$ of north side streams is similar to the maximum $ØCO_{2,Si}$ in south side streams (257×10^3 mol CO_2 km^{-2} yr^{-1}), and the largest $ØCO_{2,Si}$ observed in a north side stream (1237×10^3 mol CO_2 km^{-2} yr^{-1}) was much greater than the highest $ØCO_{2,Si}$ for south side streams (Table 3). The north side maximum $ØCO_{2,Si}$ represents a maximum possible yield as it was the greatest yield calculated from four separate samples taken from a single stream (Trib. 2 to Chajonja). The lowest calculated $ØCO_{2,Si}$ for Trib. 2 to Chajonja (473×10^3 mol CO_2 km^{-2} yr^{-1}; Table SI 3) was roughly one third of the maximum $ØCO_{2,Si}$. However, Trib. 2 to Chajonja was the only stream where $ØCO_{2,Si}$ calculated from multiple samples and discharge measurements deviated from the mean by more than 30% (38%). Moreover, the lowest calculated $ØCO_{2,Si}$ from Trib. 2 to Chajonja was still nearly twice the highest $ØCO_{2,Si}$ determined for any south side stream. In addition, the lowest $ØCO_{2,Si}$ for north side

Table 3
Median and ranges of $\alpha_{Si,rain,carb}$ and $ØCO_{2,Si}$ for north and south side streams.

	α_{Si}	α_{rain}	α_{carb}	$ØCO_{2,Si}$ (10^3 mol CO_2 km^{-2} yr^{-1})
North side streams, n = 50				
Median	91.1	5.4	2.3	260
Min	79.3	0.0	0.0	127
Max	98.1	18.3	16.1	1237
South side streams, n = 29				
Median	88.8	9.3	0.4	78
Min	31.8	0.0	0.0	11
Max	98.5	42.3	25.9	257

streams (127×10^3 mol CO_2 km^{-2} yr^{-1}) was 60% greater than the median $ØCO_{2,Si}$ for south side streams (Table 3). Clearly, the data presented in this section support the hypothesis proposed in the introduction: watersheds draining the north, wet, windward side of the Sierra de Las Minas have greater $ØCO_{2,Si}$ yields than watersheds draining the south, dry, leeward side of the range.

4. Discussion

4.1. Representativeness of $ØCO_{2,Si}$ as annual calculations

How representative are the presented $ØCO_{2,Si}$ as annual calculations? South side samples were collected during the beginning of the wet season (Fig. SI 1b), but only two precipitation events were observed during this sampling trip. The paucity of rainfall on the south side suggests that increases in discharge over baseflow are likely small and infrequent. Therefore, changes in stream chemistry associated with changes in discharge are not expected to have much effect on annual $ØCO_{2,Si}$. Thus extrapolations to annual $ØCO_{2,Si}$ from single samples is probably a reasonable representation of actual annual yields. A strong seasonality exists in the mean daily discharge of the largest north side stream sampled, R. Matanzas, from May 2003 to May 2010 that leads to at least a 5-fold increase in discharge from the dry to the wet season (Fig. SI 1a), with storm events in the wet season that caused an order of magnitude increase in discharge (Fig. SI 2). This seasonality is likely representative of all north side watersheds, and north side samples were collected and discharges measured during the dry season. Therefore, a more thorough examination of discharge effects on stream chemistry is necessary for north side streams than for south side streams.

Concentrations of Si and HCO_3^- were generally greater during the lowest discharge measured than during the highest discharge measured for a given north side stream (Table SI 2). Discharge differences between the highest and lowest discharge measured were 2 to 3-fold, but differences in Si and HCO_3^- concentrations were no more than 50% of the lowest concentration (Trib. 1 to Chajonja, Trib. 2 to Chajonja, R. Sibija; Table SI 2). For two north side streams, R. Raxon, R. Samilja, the highest Si and HCO_3^- concentrations were close to double that of the lowest concentrations. However, discharge from the R. Raxon was gauged only once and R. Samilja not at all, so these differences in chemistry cannot be compared directly to differences in discharge. Still, all evidence from comparing multiple samples and discharge measurements from the same sites suggests that potential decreases in Si and HCO_3^- concentrations from the dry to the wet season would not be greater than increases in discharge. Annual $ØCO_{2,Si}$ calculated from separate samples of the same north side stream deviated from the mean by no more than 38% (Trib. 2 to Chajonja) and mostly by less than 30%, suggesting that extrapolation from a single sample to annual $ØCO_{2,Si}$ in north side streams is representative by roughly ±30%. Lastly, a positive linear correlation exists between $ØCO_{2,Si}$ and discharge for all streams (north and south) where discharge was measured, including for $ØCO_{2,Si}$ calculated from separate north side samples of the same stream ($r^2 = 0.70$, $n = 54$; Fig. 3). If this relationship persists through the wet season on the north side of the range, then north side yields may underestimate actual annual $ØCO_{2,Si}$.

4.2. Influences of lithology and basin morphology on $ØCO_{2,Si}$

Differences in HCO_3^-:Si and TZ^+:Si among streams were attributed to lithological differences (Section 3.2), namely influences from the San Lorenzo marble and Chóchal formation compared to influences from the Santa Rosa shale and/or highly weathered

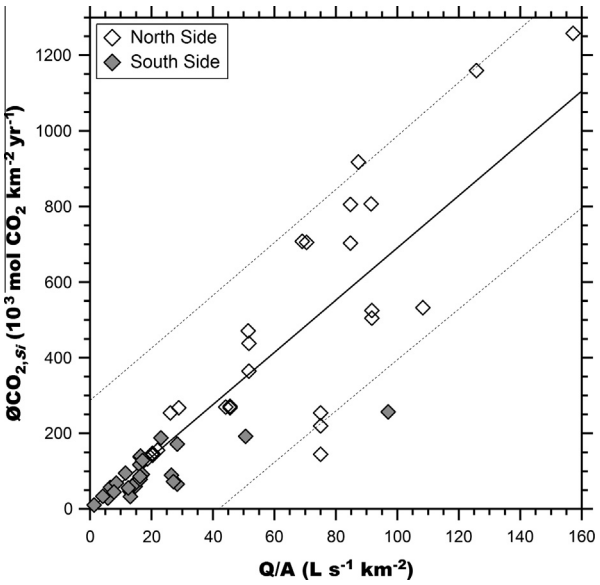

Fig. 3. $ØCO_{2,Si}$ vs. water yields for north and south side streams with measured discharge. Solid line represents a regression forced through zero ($r^2 = 0.70$, $n = 54$). Dashed lines indicate 95% confidence bands.

substrates. Low Si: HCO_3^- and Si: TZ^+ were attributed to influences from carbonate weathering, even in those watersheds without mapped carbonate bedrock. Others have observed disproportionate influences on stream chemistry from minor carbonate phases in largely silicate metamorphic rock (Jacobson et al., 2003). Unmapped carbonate rock may also be influencing the stream chemistry. No matter the cause, carbonate weathering contributions to stream chemistry were accounted for either by correcting HCO_3^- concentrations with α_{carb} or by calculating $ØCO_{2,Si}$ as 2.ØSi. The greater Si: HCO_3^- and Si: TZ^+ observed in most north side watersheds compared to most south side watersheds probably reflects highly weathered substrates and/or influences from the Santa Rosa shale underlying north side watersheds (Edmond et al., 1995; Clow and Drever, 1996; Clow and Mast, 2010), which would create positive inaccuracies in any $ØCO_{2,Si}$ calculated as 2.ØSi (Edmond and Huh, 1997; Clow and Mast, 2010). In such cases, α_{carb} corrected concentrations of HCO_3^- were thought to provide a more accurate estimate of $ØCO_{2,Si}$ and so yields were calculated as $ØALK_{Si}$. In this way, influences of secondary clay mineral weathering (i.e. Si dissolving into solution without contributing alkalinity) were accounted for. Therefore, any influence of lithology on the differences observed for $ØCO_{2,Si}$ between the north and south side of the range were thought to be mostly eliminated, and so the yields were considered reasonably as comparable as from streams draining a single lithology.

The morphology of south side basins is typically flatter and more gently sloping than north side basins. These observations were supported by the 5–10° difference in modal slope for the north compared to the south side of the Sierra de Las Minas (Section 2.1, Fig. 1c). Influences of basin morphology on chemical weathering depend on other factors such as overland flow and the balance between mineral dissolution rates, chemical equilibrium in the substrate, and water residence time (Berner, 1978, 1981; Blum and Lasaga, 1987; Lasaga et al., 1994; Steefel and Maher, 2009; Maher, 2010, 2011). A null relationship between basin slope and $ØCO_{2,Si}$ would imply longer flow paths in north side watersheds than in south side watersheds and little relationship between slope and runoff for the Sierra de Las Minas (Maher, 2011). Therefore, differences in basin morphology between the north and the south side more likely had a negative than positive

Please cite this article in press as: McAdams, B.C., et al. Two sides to every range: Orographic influences on CO_2 consumption by silicate weathering. Appl. Geochem. (2015), http://dx.doi.org/10.1016/j.apgeochem.2015.04.010

impact on the differences in $\emptyset CO_{2,Si}$ between north and south side streams (McGuire et al., 2005; Maher, 2010, 2011). The relative differences between median HCO_3^- and Si concentration from the north to the south side of the range (Section 3.2) were roughly an order of magnitude lower than the relative differences in discharge between the north and south side (Section 3.1) and probably reflect mostly chemostatic behavior (Godsey et al., 2009; Clow and Mast, 2010). $\emptyset CO_{2,Si}$ was positively correlated with water yields for all streams (Fig. 3). Mostly chemostatic behavior of stream chemistry combined with a positive correlation between $\emptyset CO_{2,Si}$ and water yields bolsters the notion that basin morphology has little influence on $\emptyset CO_{2,Si}$ in the Sierra de Las Minas and that hydrologic budget (i.e. precipitation) plays a more important role in the hypothesis that $\emptyset CO_{2,Si}$ are greater from rivers draining the wet, windward, north side of the Sierra de Las Minas than from rivers draining the dry, leeward, south side of the range.

4.3. Global context

Among mountain ranges around the world, $\emptyset CO_{2,Si}$ from streams draining the Sierra de Las Minas range from the low end of global yields on the south side of the range toward the high end of global yields on the north side of the range (Table 4). North side yields are similar to other locales with a mix of sedimentary, metamorphic, and/or igneous units such as the north and south islands of New Zealand and the Andes (Table 4). However, south side yields are more similar to those measured in the Himalayas and the highly weathered Congo (Table 4). Orographic influences have been observed to elevate chemical weathering rates on the wet, windward side of a volcanic island above those of the dry, leeward side (Gaillardet et al., 2011). Others have observed chemical fluxes positively related to discharge (Gaillardet et al., 1999; Stefánsson and Gíslason, 2001; Godsey et al., 2009). Groundwater flushing has been proposed as a dominant mechanism responsible for chemostatic behavior of watersheds with discharge, leading to a positive relationship between precipitation and chemical weathering yields (Clow and Mast, 2010). Water transport through the steeper north side catchments of the Sierra de Las Minas may be more rapid than through the less steep south side catchments (McGuire et al., 2005; Maher, 2011). However, any differences in water residence time did not overcome mineral dissolution rates so as to obscure the positive relationship between precipitation or water yields and $\emptyset CO_{2,Si}$ from the north to the south side of the range (Fig. 3). Therefore, orographically driven weathering dynamics in the Sierra de Las Minas suggest that transport was the main factor controlling solute export, and water residence time across the range was sufficient to promote increases in $\emptyset CO_{2,Si}$ with water yield (Berner, 1978; Lasaga et al., 1994; Steefel and Maher, 2009; Maher, 2010). Furthermore, the Sierra de Las Minas are known to be prone to landslide events (Restrepo and Alvarez, 2006; Restrepo et al., 2009; Ramos Scharrón et al., 2012) that break apart bedrock and redistribute fresh mineral surfaces throughout watersheds (Vitousek et al., 1997; Filipelli and Souch, 1999). Large landslide events have been tied to extreme rainfall events in the Sierra de Las Minas (Bucknam et al., 2001; Restrepo and Alvarez, 2006), and landslide activity in general can be closely tied to rainfall (Caine, 1980; Larsen and Simon, 1993; Iverson, 2000; Tsaparas et al., 2002; Collins and Znidarcic, 2004; Crosta and Frattini, 2008; Guzzetti et al., 2008). If precipitation promotes $\emptyset CO_{2,Si}$ in tropical watersheds prone to landslides, and landslides increase with precipitation and with more frequency of extreme rainfall events; then potential increases in precipitation and extreme weather associated with climate warming (O'Gorman and Schneider, 2009; Allan et al., 2010; Knutson et al., 2010; Giorgi et al., 2011) could provide a negative climate feedback mechanism in tropical mountain watersheds. Of course, such a mechanism would be closely tied to the ways in which precipitation increases influence physical weathering, basin morphology, and water–rock interactions (Clow and Mast, 2010; Maher, 2010, 2011; Maher and Druhan, 2014). A further understanding of this mechanism in the tropics would only be gained from a more extensive network of information (e.g. continuous precipitation records, continual synoptic discharge and stream chemistry measurements, physical weathering rate quantification) in remote locations affected by rain shadows (e.g. the Sierra de Las Minas).

Table 4
Global $\emptyset CO_{2,Si}$ from rivers by region.

Watershed region	$\emptyset CO_{2,Si}$ (10^3 mol CO_2 km^{-2} yr^{-1})	
Sierra de Las Minas (this study)		
North Side	(260)*	127–1237
South Side	(78)*	11–257
New Zealand		
Taranaki Region[a]		217–2926
Sedimentary and Ruapehu Region[a]		128–851
Greywacke and Argillite Region[a]		875
North Island[b]		170–1074
South Island[b]		296–946
Dominica[c]		190–1575
Martinique and Guadeloupe[d]		1100–1400
Réunion Island[e]		1300–4400
Andes[f]		220–1000
Himalayas[f]		100–320
Deccan Traps[g]		580–2540
Congo[h]		51

* Median values in parentheses.
[a] Goldsmith et al. (2008b).
[b] Lyons et al. (2005).
[c] Goldsmith et al. (2010).
[d] Rad et al. (2006).
[e] Louvat and Allègre (1997).
[f] Edmond and Huh (1997).
[g] Dessert et al. (2001).
[h] Gaillardet et al. (1995).

5. Conclusions

The rain shadow of the Sierra de Las Minas provided a natural experimental setting to isolate the effects of rainfall on $\emptyset CO_{2,Si}$ within a single mountain range. It was found that streams draining the north, wet, windward side of the range had greater $\emptyset CO_{2,Si}$ than streams draining the south, dry, leeward side of the range. Though annual yields were extrapolated from single samples, it was reasoned that these extrapolations were reasonably representative of annual $\emptyset CO_{2,Si}$. Potential influences of lithology were accounted for using major cation and silica chemistry of the streams and so lithology was thought to have little impact, if any, on calculated $\emptyset CO_{2,Si}$ yields. Similarly, mostly chemostatic behavior and a strong correlation between $\emptyset CO_{2,Si}$ and water yields, among other considerations, imply little impact, if any, of basin morphology on differences in $\emptyset CO_{2,Si}$ between north, wet and south, dry side watersheds. Therefore, precipitation (i.e. the orographic rain shadow of the Sierra de Las Minas) was considered the controlling variable on differences in $\emptyset CO_{2,Si}$ between the wet and dry sides of the range. This effect may be applicable to other tropical mountain watersheds where a rain shadow is present, and especially in those areas prone to landslides. Furthermore, a greater understanding of the influences of rain shadows on $\emptyset CO_{2,Si}$ may inform climate models as to the impact that possible changes in precipitation would have on atmospheric CO_2 consumption from silicate weathering.

Please cite this article in press as: McAdams, B.C., et al. Two sides to every range: Orographic influences on CO_2 consumption by silicate weathering. Appl. Geochem. (2015), http://dx.doi.org/10.1016/j.apgeochem.2015.04.010

Acknowledgements

Financial support for this work was provided by NSF EAR 0909271, NSF DEB 0919043, and NSF DEB 0919138. An NSF GRF supported AMT during her work on the project. Permits for work were granted under the Consejo Nacional de Areas Protegidas—CONAP—permit numbers 00378-A, 00448-A, and 00033-B. Field logistics would not have come together without the hospitality of the Droeges family and the cooperation of the Fundación Defensores de la Naturaleza. We gratefully acknowledge the help of Andi Portier and Claire Mondro, who were essential to field collection of samples and analyses; and Jeff Pigott, who provided assistance with geochemical modelling. Finally, we thank the two anonymous reviewers who provided valuable input that improved the final manuscript.

Appendix A. Supplementary material

Supplementary data associated with this article can be found, in the online version, at http://dx.doi.org/10.1016/j.apgeochem.2015.04.010.

References

Allan, R.P., Soden, B.J., John, V.O., Ingram, W., Good, P., 2010. Current changes in tropical precipitation. Environ. Res. Lett. 5 (2), 025205. http://dx.doi.org/10.1088/1748-9326/5/2/025205.

Anderson, S.P., Dietrich, W.E., Brimhall, G.H., 2002. Weathering profiles, mass-balance analysis, and rates of solute loss: linkages between weathering and erosion in a small, steep catchment. Geol. Soc. Am. Bull. 114 (9), 1143–1158.

Averbuch, O., Tribovillard, N., Devleeschouwer, X., Riquier, L., Mistiaen, B., van Vliet-Lanoe, B., 2005. Mountain building-enhanced continental weathering and organic carbon burial as major causes for climatic cooling at the Frasnian-Famennian boundary (c. 376 ma)? Terra 17 (1), 25–34. http://dx.doi.org/10.111/j.1365-3121.2004.00580.x.

Barros, A.P., Lettenmaier, D.P., 1994. Dynamic modeling of orographically induced precipitation. Rev. Geophys. 32 (3), 265–284. http://dx.doi.org/10.1029/94RG00625.

Berner, R.A., 1978. Rate control of mineral dissolution under earth surface conditions. Am. J. Sci. 278 (9), 1235–1252. http://dx.doi.org/10.2475/ajs.278.9.1235.

Berner, R.A., 1981. Kinetics of weathering and diagenesis. Rev. Mineral. 8, 111–134.

Berner, R.A., 1994. 3GEOCARB II: A revised model of atmospheric CO_2 over Phanerozoic time. Am. J. Sci. 294 (1), 56–91. http://dx.doi.org/10.2475/ajs.294.1.56.

Berner, R.A., Lasaga, A.C., Garrels, R.M., 1983. The carbonate-silicate geochemical cycle and its effect on atmospheric carbon dioxide over the past 100 million years. Am. J. Sci. 283 (7), 641–683. http://dx.doi.org/10.2475/ajs.283.7.641.

Blum, A.E., Lasaga, A.C., 1987. Monte Carlo simulations of surface reaction rate laws. In: Stumm, W. (Ed.), Aquatic Surface Geochemistry. Wiley, New York, pp. 255–292.

Bluth, G.J.S., Kump, L.R., 1994. Lithologic and climatologic controls of river chemistry. Geochim. Cosmochim. Acta 58 (10), 2341–2359. http://dx.doi.org/10.1016/0016-7037(94)90015-9.

Bonis, S., 1967. Mapa de reconocimiento geológico del cinturón plegado de Alta Verapaz, Guatemala. Guatemala Instituto Geografico Nacional. scale 1:125,000.

Bonis, S., Bohnenberger, O.H., Dengo, G., 1970. Mapa geologico de la Republica de Guatemala. Guatemala Instituto Geografico Nacional, scale 1:500,000.

Bucknam, R.C., Coe, J.A., Chavarria, M.M., Godt, J.W., Tarr, A.C., Bradley, L., Rafferty, S., Hancock, D., Dart, R.L., Johnson, M.L., 2001. Landslides Triggered by Hurricane Mitch in Guatemala—Inventory and Discussion. US Geol. Surv. Open File Report, 01–443.

Bundschuh, J., Alvarado, G.E., 2007. Central America: Geology, Resources and Hazards. Taylor and Francis, New York.

Caine, N., 1980. The rainfall intensity: duration control of shallow landslides and debris flows. Geogr. Ann. Ser. A: Phys. Geogr. 62 (1–2), 23–27.

Campbell, J.A., 1982. The Biogeography of the Cloud Forest Herpetofauna of Middle America, with Special Reference to the Sierra de Las Minas of Guatemala. Ph.D. Dissertation. University of Kansas, Lawrence, Kansas, 230 p.

Carey, A.E., Gardner, C.B., Goldsmith, S.T., Lyons, W.B., Hicks, D.M., 2005a. Organic carbon yields from small, mountainous rivers, New Zealand. Geophys. Res. Lett. 32 (15), L15404. http://dx.doi.org/10.1029/2005GL023159.

Carey, A.E., Lyons, W.B., Owens, J.S., 2005b. Significance of landscape age, uplift, and weathering rates to ecosystem development. Aquat. Geochem. 11 (2), 215–239. http://dx.doi.org/10.1007/s10498-004-5733-6.

Carey, A.E., Kao, S.J., Hicks, D.M., Nezat, C.A., Lyons, W.B., 2006. The geochemistry of rivers in tectonically active areas of Taiwan and New Zealand. Tecton. Clim. Landsc. Evol. Geol. Soc. Am. Spec. Pap. 398, 339–351. http://dx.doi.org/10.1130/2006.2398(21).

Clow, D.W., Drever, J.I., 1996. Weathering rates as a function of flow through an alpine soil. Chem. Geol. 132 (1–4), 131–141. http://dx.doi.org/10.1016/S0009-254(96)00048-4.

Clow, D.W., Mast, M.A., 2010. Mechanisms for chemostatic behavior in catchments: implications for CO_2 consumption by mineral weathering. Chem. Geol. 269, 40–51. http://dx.doi.org/10.1016/j.chemgeo.2009.09.014.

Collins, B.D., Znidarcic, D., 2004. Stability analyses of rainfall induced landslides. J. Goetech. Geoenviron. Eng. 130 (4), 362–367. http://dx.doi.org/10.1061/(ASCE)1090-024(2004) 130:4(362).

Crosta, G.B., Frattini, P., 2008. Rainfall-induced landslides and debris flows. Hydrol. Process. 22 (4), 473–477. http://dx.doi.org/10.1002/hyp.6885.

Dessert, C., Dupré, B., François, L.M., Schott, J., Gaillardet, J., Chakrapani, G., Bajpai, S., 2001. Erosion of Deccan Traps determined by river geochemistry: impact on the global climate and the $^{87}Sr/^{86}Sr$ ratio of seawater. Earth Planet. Sci. Lett. 188 (3–4), 459–474. http://dx.doi.org/10.1016/S0012-821X(01)00317-X.

Edmond, J.M., Huh, Y., 1997. Chemical weathering yields from basement and orogenic terrains in hot and cold climates. In: Ruddiman, W.F. (Ed.), Tectonic Uplift and Climate Change. Plenum Press, New York, pp. 329–351.

Edmond, J.M., Palmer, M.R., Measures, C.I., Grant, B., Stallard, R.F., 1995. The fluvial geochemistry and denudation rate of the Guayana Shield in Venezuela, Colombia, and Brazil. Geochim. Cosmochim. Acta 59 (16), 3301–3325. http://dx.doi.org/10.1016/0016-7037(95)00128-M.

Filipelli, G.M., 1997. Intensification of the Asian monsoon and a chemical weathering event in the late Miocene early Pliocene: implications for late Neogene climate change. Geology 25 (1), 27–30. http://dx.doi.org/10.1130/0091-7613(1997) 025<0027:IOTAMA>2.3.CO;2.

Filipelli, G.M., Souch, C., 1999. Effects of climate and landscape development on the terrestrial phosphorous cycle. Geology 27 (2), 171–174. http://dx.doi.org/10.1130/0091-7613(1999) 027<0171:EOCALD>2.3.CO;2.

Francois, L.M., Walker, J.C.G., 1992. Modelling the Phanerozoic carbon cycle and climate: constraints from the $^{87}Sr/^{86}Sr$ isotopic ratio of seawater. Am. J. Sci. 292 (2), 81–135. http://dx.doi.org/10.2475/ajs.292.2.81.

Gaillardet, J., Dupré, B., Allègre, C.J., 1995. A global geochemical mass budget applied to the Congo basin rivers: erosion rates and continental crust composition. Geochim. Cosmochim. Acta 59 (17), 3469–3485. http://dx.doi.org/10.1016/0016-7037(95)00230-W.

Gaillardet, J., Dupré, B., Louvat, P., Allègre, C.J., 1999. Global silicate weathering and CO_2 consumption rates deduced from the chemistry of large rivers. Chem. Geol. 159 (1–4), 3–30. http://dx.doi.org/10.1016/S0009-2541(99)00031-5.

Gaillardet, J., Rad, S., Rive, K., Louvat, P., Gorge, C., Allègre, C.J., Lajeunesse, E., 2011. Orography-driven chemical denudation in the Lesser Antilles: evidence for a new feed-back mechanism stabilizing atmospheric CO_2. Am. J. Sci. 311 (10), 851–894. http://dx.doi.org/10.2475/10.2011.02.

Galewsky, J., 2009. Rain shadow development during the growth of mountain ranges: an atmospheric dynamics perspective. J. Geophys. Res. – Earth Surf. 114, F01018. http://dx.doi.org/10.1029/2008JF001085.

Garrels, R.M., 1967. Genesis of some ground waters from igneous rocks. In: Abelson, P.H. (Ed.), Researches in Geochemistry, vol. 2. John Wiley, New York, pp. 405–420.

Giorgi, F., Im, E.S., Coppola, E., Diffenbaugh, N.S., Gao, X.J., Mariotti, L., Shi, Y., 2011. Higher hydroclimatic intensity with global warming. J. Clim. 24, 5309–5324. http://dx.doi.org/10.1175/2011JCLI3979.1.

Goldsmith, S.T., Carey, A.E., Lyons, W.B., Kao, S.J., Lee, T.Y., Chen, J., 2008a. Extreme storm events, landscape denudation, and carbon sequestration: Typhoon Mindulle, Choshui River, Taiwan. Geology 36 (6), 483–486. http://dx.doi.org/10.1130/G24624A.1.

Goldsmith, S.T., Carey, A.E., Lyons, W.B., Hicks, D.M., 2008b. Geochemical fluxes and weathering of volcanic terrains on high standing islands: Taranaki and Manawatu-Wanganui regions of New Zealand. Geochim. Cosmochim. Acta 72 (9), 2248–2267. http://dx.doi.org/10.1016/j.gca.2007.12.024.

Goldsmith, S.T., Carey, A.E., Johnson, B.M., Welch, S.A., Lyons, W.B., McDowell, W.H., Pigott, J.S., 2010. Stream geochemistry, chemical weathering and CO_2 consumption potential of andesitic terrains, Dominica, Lesser Antilles. Geochim. Cosmochim. Acta 74 (1), 85–103. http://dx.doi.org/10.1016/j.gca.2009.10.009.

Godsey, S.E., Kirchner, J.W., Clow, D.W., 2009. Concentration-discharge relationships reflect chemostatic characteristics of US catchments. Hydrol. Proc. 23 (13), 1844–1864. http://dx.doi.org/10.1002/hyp.7315.

Guzzetti, F., Peruccacci, S., Rossi, M., Stark, C.P., 2008. The rainfall intensity–duration control of shallow landslides and debris flows: an update. Landslides 5 (1), 3–17. http://dx.doi.org/10.1007/s10346-007-0112-1.

Holder, C.D., 2006. The hydrological significance of cloud forests in the Sierra de Las Minas biosphere reserve, Guatemala. Geoforum 37 (1), 82–93. http://dx.doi.org/10.1016/j.geoforum.2004.06.008.

Houze, R.A., 2012. Orographic effects on precipitating clouds. Rev. Geophys. 50, RG1001. http://dx.doi.org/10.1029/2011RG000365.

Iverson, R.M., 2000. Landslide triggering by rain infiltration. Water Resour. Res. 36 (7), 1897–1910. http://dx.doi.org/10.1029/2000WR900090.

Jacobson, A.D., Blum, J.D., 2003. Relationship between mechanical erosion and atmospheric CO_2 consumption in the New Zealand southern alps. Geology 31 (10), 865–868. http://dx.doi.org/10.1130/G19662.1.

Jacobson, A.D., Blum, J.D., Chamberlain, C.P., Craw, D., Koons, P.O., 2003. Climatic and tectonic controls on chemical weathering in the New Zealand southern alps. Geochim. Cosmochim. Acta 67 (1), 29–46. http://dx.doi.org/10.1016/S0016-7037(02)01053-0.

Knutson, T.R., McBride, J.L., Chan, J., Emanuel, K., Holland, G., Landsea, C., Held, I., Kossin, J.P., Srivastava, A.K., Sugi, M., 2010. Tropical cyclones and climate change. Nat. Geosci. 3, 157–163. http://dx.doi.org/10.1038/ngeo779.

Larsen, M.C., Simon, A., 1993. A rainfall intensity–duration threshold for landslides in a humid-tropical environment, Puerto Rico. Geogr. Ann. Ser. A: Phys. Geogr. 75 (1–2), 13–23.

Lasaga, A.C., Soler, J.M., Ganor, J., Burch, T.E., Nagy, K.L., 1994. Chemical weathering rate laws and global geochemical cycles. Geochim. Cosmochim. Acta 58 (10), 2361–2386. http://dx.doi.org/10.1016/0016-7037(94)90016-7.

Louvat, P., Allègre, C.J., 1997. Present denudation rates on the island of Réunion determined by river geochemistry: basalt weathering and mass budget between chemical and mechanical erosions. Geochim. Cosmochim. Acta 61 (17), 3645–3669. http://dx.doi.org/10.1016/S0016-7037(97)00180-4.

Lyons, W.B., Nezat, C.A., Carey, A.E., Hicks, D.M., 2002. Organic carbon fluxes to the ocean from high-standing islands. Geology 30 (5), 443–446. http://dx.doi.org/10.1130/0091-7613(2002) 030<0443:OCFTTO>2.0.CO;2.

Lyons, W.B., Carey, A.E., Hicks, D.M., Nezat, C.A., 2005. Chemical weathering in high-sediment-yielding watersheds, New Zealand. J. Geophys. Res. – Earth Surf. 110 (F1), F01008. http://dx.doi.org/10.1029/2003JF000088.

Maher, K., 2010. The dependence of chemical weathering rates on fluid residence time. Earth Planet. Sci. Lett. 294 (1–2), 101–110. http://dx.doi.org/10.1016/j.epsl.2010.03.010.

Maher, K., 2011. The role of fluid residence time and topographic scales in determining chemical fluxes from landscapes. Earth Planet. Sci. Lett. 312 (1–2), 48–58. http://dx.doi.org/10.1016/j.epsl.2011.09.040.

Maher, K., Druhan, J., 2014. Relationships between the transit time of water and the fluxes of weathered elements through the critical zone. Procedia Earth Planet. Sci. 10, 16–22. http://dx.doi.org/10.1016/j.proeps.2014.08.004.

McAdams, B.C., 2012. Chemical Weathering and Organic Carbon Transport in an Active Mountain Belt: Sierra de Las Minas, Guatemala. Master's Thesis. The Ohio State University, Columbus, OH, 114 p.

McGuire, K.J., McDonnell, J.J., Weiler, M., Kendall, C., McGlynn, B.L., Welker, J.M., Seibert, J., 2005. The role of topography on catchment-scale water residence time. Water Resour. Res. 41 (5), W05002. http://dx.doi.org/10.1029/2004WR003657.

Menking, J.A., Han, J.W., Gasparini, N.M., Johnson, J.P.L., 2013. The effects of precipitation gradients on river profile evolution on the Big Island of Hawai'i. Geol. Soc. Am. Bull. 125 (3–4), 594–608. http://dx.doi.org/10.1130/B30625.1.

Milliman, J.D., Syvitski, J.P.M., 1992. Geomorphic/tectonic control of sediment discharge to the ocean: importance of small mountainous rivers. J. Geol. 100 (5), 525–544.

Millot, R., Gaillardet, J., Dupré, B., Allègre, C.J., 2002. The global control of silicate weathering rates and the coupling with physical erosion: new insights from rivers of the Canadian Shield. Earth Planet. Sci. Lett. 196 (1–2), 83–98. http://dx.doi.org/10.1016/S0012-821X(01)00599-4.

Newcomb, W.E., 1975. Geology, Structure, and Metamorphism of the Chuacus Group, Río Hondo Quadrangle and Vicinity, Guatemala. Ph.D. Dissertation. S.U.N.Y. Binghamton, Binghamton, New York, 115 p.

O'Gorman, P.A., Schneider, T., 2009. The physical basis for increases in precipitation extremes in simulations of 21st-century climate change. Proc. Natl. Acad. Sci. U.S.A. 106 (35), 14773–14777. http://dx.doi.org/10.1073/pnas.0907610106.

Rad, S., Louvat, P., Gorge, C., Gaillardet, J., Allègre, C.J., 2006. River dissolved solid loads in the Lesser Antilles: new insight into basalt weathering processes. J. Geochem. Explor. 88 (1–3), 308–312. http://dx.doi.org/10.1016/j.gexplo.2005.08.063.

Ramos Scharrón, C.E., Castellanos, E.J., Restrepo, C., 2012. The transfer of modern organic carbon by landslide activity in tropical montane ecosystems. J. Geophys. Res. – Biogeosci. 117 (G3), G03016. http://dx.doi.org/10.1029/2011JG001838.

Rantz, S.E., 1982. Measurement and Computation of Streamflow, vols. 1 and 2. U.S. Geol. Surv. Water-Supply Paper 2175.

Raymo, M.E., 1994. The Himalayas, organic-carbon burial, and climate in the Miocene. Paleoceanography 9 (3), 399–404. http://dx.doi.org/10.1029/94PA00289.

Raymo, M.E., Ruddiman, W.F., 1992. Tectonic forcing of late Cenozoic climate. Nature 359 (6391), 117–122. http://dx.doi.org/10.1038/359117a0.

Restrepo, C., Alvarez, N., 2006. Landslides and their contribution to land-cover change in the mountains of Mexico and Central America. Biotropica 38 (4), 446–457. http://dx.doi.org/10.1111/j.1744-7429.2006.00178.x.

Restrepo, C., Walker, L.R., Shiels, A.B., Bussmann, R., Claessens, L., Fisch, S., Lozano, P., Negi, G., Paolini, L., Poveda, G., Ramos-Scharrón, C., Richter, M., Velazquez, E., 2009. Landsliding and its multiscale influence on mountainscapes. Bioscience 59 (8), 685–698. http://dx.doi.org/10.1525/bio.2009.59.8.10.

Riebe, C.S., Kirchner, J.W., Granger, D.E., Finkel, R.C., 2001. Strong tectonic and weak climatic control of long-term chemical weathering rates. Geology 29 (6), 511–514. http://dx.doi.org/10.1130/0091-7613(2001) 029<0511:STAWCC>2.0.CO;2.

Riebe, C.S., Kirchner, J.W., Finkel, R.C., 2004. Erosional and climatic effects on long-term chemical weathering rates in granitic landscapes spanning diverse climate regimes. Earth Planet. Sci. Lett. 224 (3–4), 547–562. http://dx.doi.org/10.1016/j.epsl.2004.04.019.

Roe, G.H., Montgomery, D.R., Hallet, B., 2002. Effects of orographic precipitation variations on the concavity of steady-state river profiles. Geology 30 (2), 143–146. http://dx.doi.org/10.1130/0091-7613(2002) 030<0143:EOOPVO>2.0.CO;2.

Sayama, T., McDonnell, J.J., 2009. A new time–space accounting scheme to predict stream water residence time and hydrograph source components at the watershed scale. Water Resour. Res. 45 (7), W07401. http://dx.doi.org/10.1029/2008WR007549.

Soulsby, C., Tetzlaff, D., Rodgers, P., Dunn, S., Waldron, S., 2006. Runoff processes, stream water residence times and controlling landscape characteristics in a mesoscale catchment: an initial evaluation. J. Hydrol. 325, 197–221. http://dx.doi.org/10.1016/j.hydrol.2005.10.024.

Stallard, R.F., Edmond, J.M., 1983. Geochemistry of the Amazon: 2. The influence of geology and the weathering environment on the dissolved load. J. Geophys. Res. – Ocean Atmos. 88 (NC14), 9671–9688. http://dx.doi.org/10.1029/JC088iC14p09671.

Steefel, C.I., Maher, K., 2009. Fluid–rock interaction: a reactive transport approach. Rev. Mineral. Geochem. 70 (1), 485–532. http://dx.doi.org/10.2138/rmg.2009.70.11.

Stefánsson, A., Gíslason, S.R., 2001. Chemical weathering of basalts, southwest Iceland: effect of rock crystallinity and secondary minerals on chemical fluxes to the ocean. Am. J. Sci. 301 (6), 513–556. http://dx.doi.org/10.2475/ajs.301.6.513.

Stewart, B.W., Capo, R.C., Chadwick, O.A., 2001. Effects of rainfall on weathering rate, base cation provenance, and Sr isotope composition of Hawaiian soils. Geochim. Cosmochim. Acta 65 (7), 1087–1099. http://dx.doi.org/10.1016/S0016-7037(00)00614-1.

Trierweiler, A.T., 2010. The Role of Landsliding in Fluvial Carbon Transport. Master's Thesis. The Ohio State University. Columbus, OH, 120 p.

Tsaparas, I., Rahardjo, H., Toll, D.G., Leong, E.C., 2002. Controlling parameters for rainfall-induced landslides. Comput. Geotech. 29 (1), 1–27. http://dx.doi.org/10.1016/S0266-352X(01)00019-2.

Vitousek, P.M., Chadwick, O.A., Crews, T.E., Fownes, J.H., Hendricks, D.M., Herbert, D., 1997. Soil and ecosystem development across the Hawaiian Islands. GSA Today 7, 1–8.

Welch, K.A., Lyons, W.B., Whisner, C., Gardner, C.B., Gooseff, M.N., McKnight, D.M., Priscu, J.C., 2010. Spatial variations in the geochemistry of glacial meltwater streams in the Taylor Valley, Antarctica. Antarct. Sci. 22 (06), 662–672.

West, A.J., 2012. Thickness of the chemical weathering zone and implications for erosional and climatic drivers of weathering and for carbon-cycle feedbacks. Geology 40 (9), 811–814. http://dx.doi.org/10.1130/G33041.1.

West, A.J., Galy, A., Bickle, M., 2005. Tectonic and climatic controls on silicate weathering. Earth Planet. Sci. Lett. 235 (1–2), 211–228. http://dx.doi.org/10.1016/j.epsl.2005.03.020.

Weyl, R., 1980. Geology of Central America, second ed. Gebr. Borntraeger, Berlin.

Willett, S.D., 1999. Orogeny and orography: the effects of erosion on the structure of mountain belts. J. Geophys. Res. - Solid Earth 104 (B12), 28957–28981. http://dx.doi.org/10.1029/1999JB900248.

Please cite this article in press as: McAdams, B.C., et al. Two sides to every range: Orographic influences on CO_2 consumption by silicate weathering. Appl. Geochem. (2015), http://dx.doi.org/10.1016/j.apgeochem.2015.04.010